

Effect of Electrical Conductivity on Atomization Characteristics of Electrospray

J. Y. Kim and J. G. Hong[†]

School of Mechanical Engineering, Kyungpook National University, Bukgu, Daegu 41566 Republic of Korea

[†]Corresponding Author Email: jghong70@knu.ac.kr

(Received January 20, 2022; accepted May 20, 2022)

ABSTRACT

This study experimentally investigated various spraying modes in electrospraying, an atomization method in which a high voltage is applied to the auxiliary device at the tip of the nozzle. The spraying modes were generated depending on the experimental parameters (voltage, current, and flow rate) and characteristics of two test solutions (S and C), which were a mixture of ethanol, glycerol, citric acid, and water. Solution C had a higher electrical conductivity than solution S. Eleven spray modes were identified in the study. From a comparison of the spray modes, a maximum Sauter mean diameter (SMD) of the cone jet of solution S was 1.7 times that of solution S. The standard deviation of SMD for the unstable, rotating-jet, and pulsed-jet modes were more than two times that for the cone-jet mode. With an increase in flow rate in the cone jet, the SMD and SMD standard deviation of solution C increased linearly, and the SMD value of solution C was ~5% lower than that of solution B. The SMD standard deviations for both S and C solutions were small at low flow rates, and the standard deviation for solution C (with high conductivity) was smaller than that of solution S. For a given SMD, the current associated with solution C was higher than that associated with solution S. The study presented the comprehensive data for SMD, SMD standard deviation, and current in an electrospray system for the two fluids of different electrical conductivities under various experimental conditions.

Keywords: Electrospray, Conductivity, Wide cone jet; Sauter mean diameter; Standard deviation, SMD-current.

NOMENCLATURE

d	droplet size	γ	surface tension
r^*	electrical characteristic length	Q	flow rate
R_0	nondimensional flow rate	ε	permittivity
K	electrical conductivity	ε_0	dielectric constant
ρ	density		

1. INTRODUCTION

Atomization is a method of breaking up a liquid into fine particles through spraying and has applications in liquid-propellant systems, pesticide spraying, etc. Nozzles for combustion include pressure-type nozzles, which dissipate fuel using pressure, and air-assisted nozzles (Lefebvre *et al.* 2017). For ultrasonic spraying and electrospraying, microdroplets are generated using ultrasonic waves and a high voltage (rather than pressure), respectively, using an auxiliary atomization tool. In electrospray systems, the liquid is atomized using a potential difference; unlike ultrasonic spraying, electrospraying can generate uniform droplets (Sultan *et al.* 2011).

An electrospray system uses an electrical signal, enhancing the response and reproducibility compared with other spraying systems, even when the spraying conditions change (flowrate, nozzle diameter, etc). Owing to these attributes, droplet size and movement can be easily controlled by manipulating the external environment (Rahmanpour and Ebrahimi 2017). In addition, electric charges on the droplet surface generate a repulsive force (owing to the electric field), thereby preventing coalescence of the generated droplets. Uniform droplets can be obtained by electrospraying (Gamero-Castano and Hruby 2001). Furthermore, the scattering of droplets is reduced because an electric field is generated between the nozzle and substrate (Basak *et al.* 2007). Based on these attributes, electrospray systems can be applied in

mass spectrometry, ion supply, or pulmonary drug delivery. Electro spray systems are used in various industries where filtration and dust collection devices are used for fine dust removal and nanofilm production. In particular, considering environmental protection, air purification technology using eco-friendly technology, which simultaneously reduces fine dust, NO_x, and SO_x using electro spray spray patterns, has been studied (Rahman *et al.* 2013). Furthermore, electro spraying technology is used to collect fine dust in subways and enclosed spaces using the active surface area of droplets. Consider the case of water. When the droplet size is reduced to less than 20 μm, the water spontaneously divides into hydrogen ions and hydroxide ions, and hydroxyl radicals are converted to hydrogen peroxide by a high electric field. Therefore, water can capture floating bacteria and viruses that are oxidized by ozone (without a filter). To take advantage of these properties, studies focused on the patterns of the spray and droplet diameter of electrostatic spraying are essential (Jeong *et al.* 2020).

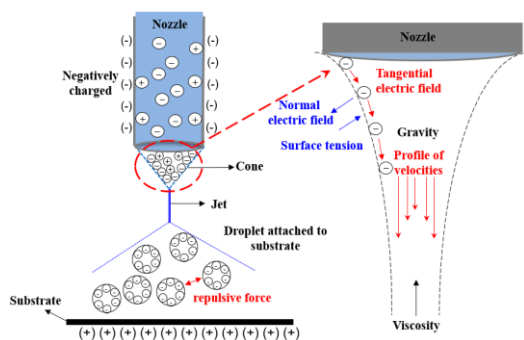


Fig. 1 Electro spray mechanism.

Figure 1 shows the operating mechanism of the electro spraying process. The nozzle is charged with the negative pole by a high voltage, and the positive ions of the fluid in the nozzle move toward the outlet. The charged liquid is accelerated as negative ions move to the surface of the fluid owing to charge separation in front of the nozzle tip. Under a high voltage (above a certain level) and given surface tension conditions, the spray pattern forms a cone with a theoretical half angle of 49.3° from the axial direction of the nozzle tip. At the surface of the cone, the ions are tangentially accelerated. The fluid accelerated to the cone tip is transformed into a jet under the influence of surface shear stress at the tip and then split into droplets owing to external disturbances (Tara Liyanage *et al.* 2018; Taylor 1964). No polymerization or combination (through surface anions) of the split droplets is observed. Regarding the cone mechanism, the shape of the cone is formed when the electric field (voltage) and surface tension in the normal direction of the fluid surface are parallel. In addition, sufficient charge relaxation time and equal charge distribution are required for the cone jet. The charge flows in the tangential direction of the fluid surface and the downward direction of the spray. Gravity acts along the direction of spraying, whereas the viscous force acts along the opposite direction (Sultan *et al.* 2011;

Taylor 1964; Kim *et al.* 2021). Previous studies on electro spray systems have majorly focused on the cone-jet mode (Sultan *et al.* 2011). Compared with other electro spray modes, this mode exhibits superior stability and continuity and enhances the uniformity in droplet size. This mode is capable of particle and droplet generation (the size of droplets varies from several nanometers to several tens of nm) (Gamero-Castano and Hruby 2001; Wang and John 2010). Compared with general pressure spraying, the electro spray process is characterized by various spraying modes depending on the experimental parameters and fluid properties. These modes are broadly divided into dripping, cone-jet, and multi jet modes. If the experimental parameters and fluid properties are changed, up to 12 modes (micro-dripping, spindle mode, wide-cone-jet mode, pulsed-jet mode, ramified-jet mode, tilted-jet mode, rotated-jet mode, and unstable mode) are observed (Cai *et al.* 2021; Jaworek and Krupa 1996; Laonual 2006).

The spray pattern of electro spray is more diverse than that of a general pressure spray nozzle, and the spray characteristics are different for each mode (Sultan *et al.* 2011). In addition, for a given spray mode, the extent of development varies with the voltage and flow conditions. Therefore, the spraying properties associated with the starting condition (where the mode is formed) differ from those corresponding to the condition immediately preceding the transition to another mode, and hence, clarification of the mode. In particular, during the cone-jet mode (a well-established electro spray mode), the changes in the spraying pattern occurring within the mode are unclear; therefore, errors are inevitable in the data obtained in this mode (Chen. *et al.* 2005).

The electrical conductivity of the solution has a significant influence on the formation and development of the electro spray mode. Moreover, conductivity plays a key role in the formation of the atomization mode and the voltage-induced changes in this mode (Eduardo *et al.* 2020).

Borra *et al.* (1999) confirmed that an increase in conductivity delayed the applied voltage of a cone jet. Moreover, Tang and Gomez (1996) reported that an increase in the conductivity decreased the charge resistance; hence, the cone-jet mode occurred at a low voltage. In addition, Ku *et al.* (2002) confirmed that the charge relaxation time was shortened, and the cone-jet mode range was narrowed. Tang and Gomez (1996) reported that the jet thickness decreased (i.e., the droplet size decreased) with an increase in conductivity, and Yazdekhashti *et al.* (2019) reported that fine droplets were generated at high conductivity levels.

In electro spray systems, the solution flow rate has a significant influence on the atomization and atomization modes at a given voltage condition. Morad *et al.* (2016) reported that the spray mode was delayed and the droplet size increased as the flow rate increased. Ganan-Calvo (1991) verified that the droplet size distribution was superior at a specific flow rate. The results of these studies suggest that, for a given volumetric flow rate, two variables

Table 1 Solution agitation data

Solution	Density (kg/m ³)	Conductivity (μs/cm)	Viscosity (m·Pas)	Surface tension (mN/m)	Permittivity
S Ethanol 72 wt.% Glycerol 18 wt.% Citric acid 10 wt.%	940	11.6	4.18	25.54	42.3
C Ethanol 66.4 wt.% Glycerol 13.3 wt.% Citric acid 20.3 wt.%	955	19.9	4.18	26.26	47.5

(voltage and flow rate) have a dominant effect on the amount of charge. Therefore, the changes in the atomization mode and droplet size associated with the mode can be controlled by manipulating these variables.

Sugiyama *et al.* (2011) reported that the nozzle-to-substrate distance (NTS) and nozzle diameter are important experimental variables. These variables can affect the mode change and droplet characteristics of the mode.

For a given volumetric flow rate, the amount of charge increases with increasing current and can therefore affect the development of the electrospray mode. Yunhua *et al.* (2019) confirmed the occurrence of the atomization mode through changes in the current and visualization of the mode. Asep *et al.* (2013) demonstrated that, for a given set of experimental conditions, the thickness of the jet decreased with increasing current. Therefore, a study focusing on the current-induced changes in the atomization mode and atomization characteristics is warranted. Studies on the effect of current on atomization are inadequate; the correlation between current and droplet size should be developed for clarity.

Therefore, in this study, we investigated the spray characteristics of solutions with different conductivities using a laboratory-scale electrospray system. The criterion for the cone-jet mode concerning fluid properties and spray conditions remains unclear, leading to contradictory results among various studies. This problem can be addressed by subdividing the range that encompasses the start and end of the mode.

In addition, the results obtained from the theoretical formulas proposed in previous studies were compared with those of droplet measurements performed in this study. The effects of the flow conditions and solution conductivity on the spray properties were investigated. As such, the effects of the three variables (electrical conductivity, voltage, and current) on the mode development and delay of the electrospray, and the spray characteristics associated with a given mode were considered.

2. MATERIALS AND METHODS

2.1 Materials

In this study, the quantity of glycerol, ethanol, and citric acid in the solution were adjusted to modify the

physical properties (except for the conductivity) of the solution. These liquids were the only substances that constituted the two working fluids, thereby verifying the characteristics associated with conductivity.

To prepare the solution, glycerin (99%, Ducksan), ethyl alcohol (94%, Ducksan), and citric acid monohydrate (99.5%, Purists, fulfills the requirements of Ph. Eur., BP, USP, E330, Sigma-Aldrich) were stirred. The stirring was performed using a multi-heating magnetic stirrer (S07-72-050, Mi-Sung) (Kim *et al.* 2021). Stirring was performed at 40 rpm and room temperature (fixed at 25 °C) for ~12 h. The stirring prepared the solution because of the high solubility of glycerol and citric acid in ethanol (this solubility results from the OH-hydrophilic group of the solution) (Jayasinghe *et al.* 2002).

2.2 Measurement of Fluid Properties

The following instruments were utilized to measure the fluid properties. A conductivity meter (CON 150) was used to measure the electrical conductivity, which was 111.8 mS/cm for the corrective solution. A kinematic viscometer (SV-10) and dynamic contact angle analyzer (DCA-200) were used to measure the viscosity and surface tension, respectively. The dielectric constant was measured using a liquid-dielectric-constant-meter (Model 871) (Kim *et al.* 2021). The components of each solution are listed in Table 1.

2.3 Experimental Setup

Figure 2 shows the installation of laboratory-scale equipment to determine the electrospraying characteristics of, such as spray patterns and currents during spraying.

A nozzle, substrate, cover, and fluid supply part were set up, as shown in the figure. To supply voltage on the nozzle, a high-voltage power supply (Korea Switching, B150; applied range: 30 kV, 15 mA) was used, and the nozzle was charged with a negative electrode to minimize hysteresis (Kim and Hong 2020). A syringe pump (NE-1000 model) was used, and the syringe (HSW Norm - Ject) had a capacity of 1 cc. A radial nozzle (single plastic nozzle, NNC-PN 21-34GA) was employed (Kim and Hong 2020). A cylindrical substrate (D:70 mm, H:10 mm) charged with a positive electrode was machined and protected by acrylic panels from outside interference such as dust and air. Support jacks (Dong Yang Science,

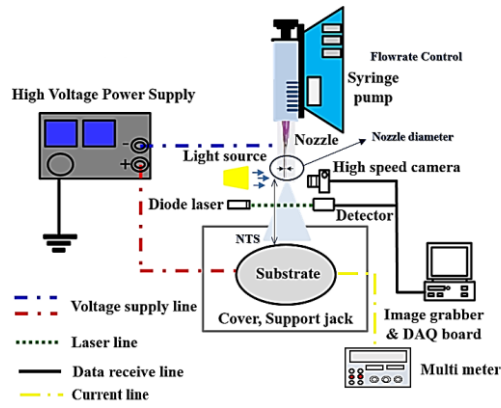


Fig. 2 Schematic of the experimental setup.

H:30 cm) supporting the protection cover facilitated adjusting the distance between the nozzle and substrate. (Wang *et al.* 2018). A high-speed camera (Phantom VEO E310L, maximum resolution: 512×512 , and sample rate: 11,500 frames/s) and a stroboscope were used to visualize and record the spraying modes (Kim *et al.* 2021). Recordings were made after the relaxation time, leading to static spraying modes and visualization for each condition. More than 150 images were analyzed for each experimental condition, and three lighting sources were deployed to record the patterns. Two of them cast light at the front, and the remaining one was positioned at the back. The front light increased the resolution of the spray mode profile and overall shape, while the light at the back assisted in acquiring the droplet shape details (Kim *et al.* 2021). The Sauter mean diameter (SMD) of the droplets sprayed from the nozzle and the SMD standard deviations were determined using a measuring device (MLXA-A12-635-5) based on the laser diffraction technique (Malvern-type) (Ku *et al.* 2015; Ariyapadi *et al.* 2001). A multimeter (DMM650, KEITHLEY) was used to measure the current. During the experiment, images were acquired at 1,000 frames/s was using the Phantom Camera Control software.

2.4 Experimental Condition

Table 2 summarizes the parameter conditions. The experiment was conducted 50 times for each condition, and the data were averaged. Nozzle diameters of 0.2, 0.4, 0.5, 0.7, and 1.0 mm (nozzle gauge: 17, 19, 21, 22, and 27) were employed for the experiments (Kim and Hong 2020). Furthermore, the NTS was increased in 10-mm intervals for values ranging from 10 mm to 50 mm. By increasing voltage from 0 kV to 15 kV continuously, spray

Table 2 Experimental condition

Condition	Value
Nozzle diameter (mm)	0.2, 0.4, 0.5, 0.7, 1.0
NTS (mm)	10, 20, 30, 40, 50
Flow rate (mL/h)	0.3, 0.6, 0.9, 1.2, 1.5, 1.8, 2.1, 3.0, 6.0
Ambient temperature (°C)	25
Relative humidity (%)	40 ± 10

modes without hysteresis were recorded. The effect of flow rate was investigated by increasing the rate in 0.3-mL/h intervals for values ranging from 0.3–6.0 mL/h. To minimize the change in spray pattern and droplet characteristics by external effects, the experiment was conducted at room temperature of 25°C, with humidity maintained at $40 \pm 10\%$.

3. RESULTS

3.1 Spray Image of Electrospray

Figure 3 shows the spray mode associated with the increase in the voltage and flow rate under a given set of electrospray test conditions. These results confirmed that 11 modes were generated as the voltage and flow rate increased (Laounal 2006). The microdripping mode occurred under low-flow-rate conditions, where the droplet size was similar to the external nozzle diameter. The dripping mode occurs under high-flow-rate conditions. Unlike gravity, the electric field had a marginal effect on the dripping mode, where the droplet size was 1.89 times the nozzle diameter. The microdripping, spindle, wide-cone-jet, and cone-jet modes (in the order of spray mode development) were generated as the applied voltage increased, regardless of the flow condition.

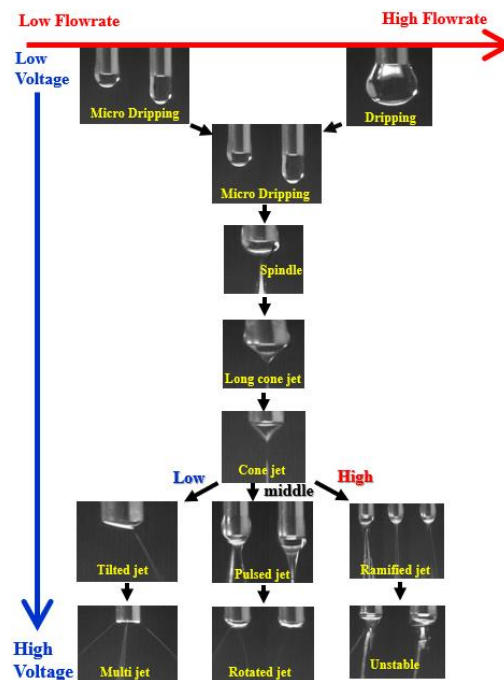


Fig. 3 Spray image of electrospray.

In the spindle mode, a cone was formed from the nozzle tip, but no jet was formed from the cone tip, and the liquid filament disintegrated into droplets.

Thus, this mode represents a transition state between the dripping and cone-jet modes. The spray pattern of the wide cone jet resembled that of the cone jet, but the cone axis and jet were both longer than the nozzle. The cone jet displayed the most stable pattern among the spray modes, with a half-angle similar to

the theoretical 49.3° reported by [Tang and Gomez \(1996\)](#).

After the occurrence of the cone jet, the spray-mode development process differed with flow rate. Cones and jets were formed when a tilted jet was subjected to low-flow-rate conditions (<1.2 mL/h).

The tilted jet displayed two differences compared to the cone jet. The tilted jet was oriented to one side and displayed an unstable profile when the jet split.

This may have resulted from the dominance of the electric field acting predominantly in the normal and tangential directions of the fluid surface, owing to the high voltage at the tip of the jet.

Increasing the voltage yielded a multi-jet. In the multi-jet mode, jets were simultaneously formed and sprayed in several directions from the nozzle tip. The number of jets was high under high flow rate and high voltage conditions. This resulted from the fact that the voltage acting in the perpendicular direction of the fluid surface exceeded the surface tension of the fluid, resulting in cone contraction and making several branches of jets on the cone surface.

Under medium-flow-rate conditions (<3.0 mL/h), a higher voltage than the voltage during the formation of the cone-jet mode produced a pulsed jet. A rotating jet was resulted when the voltage was further increased. The pulsed-jet mode has both cones and jets. In the pulsed-jet mode, pulsation-induced periodic changes along the axial direction were observed in cones and jets. The pulsed jet appears as a spindle shape with a cone shape maintained at a specific flow rate and voltage ([Cai et al. 2021](#)). This was particularly true for the rotating-jet mode, where several cones and jets were rotated counterclockwise. During the rotating jet, the cone shape is maintained while the cone rotates, owing to the unique combination of surface tension, centrifugal force, and viscous force ([Suhendi et al. 2013](#)). For high-flow-rate conditions (<6.0 mL/h), the ramified-jet mode and unstable mode appeared when the voltage was increased after the occurrence of the cone-jet mode. The ramified-jet mode formed a cone shape; however, the jet was torn into several branches. In the unstable mode, cone and jet formation were impossible because of the high flow rate and electric field during spraying, and the spray pattern was unstable ([Ting et al. 2013](#)).

3.2 Current Data

Figures 4–7 show the dependence of the current on voltage, flow rate, nozzle diameter, and NTS. Figure 4 shows the effect of the applied voltage on the current level of the S and C solutions and the range in which the cone shape is formed. Current values were obtained when they exceeded the threshold of the ammeter. For the C solution, which had a higher electrical conductivity than the S solution, the current increased significantly with an increase in voltage before the formation of the cone jet. The current value was constant in the wide-cone-jet and the cone-jet modes when the shape of the cone jet was stable. The range corresponding to the cone shape formation was similar to that of the

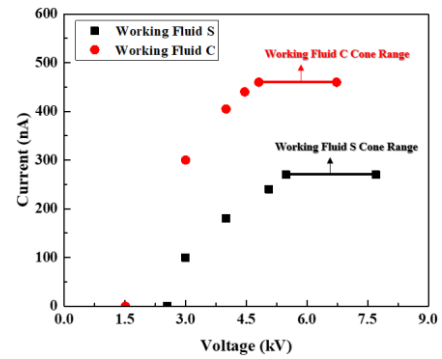


Fig. 4. Dependence of the current associated with the S and C solutions on the voltage (nozzle diameter: 0.5 mm, NTS: 30 mm, and flow rate: 3.0 mL/h).

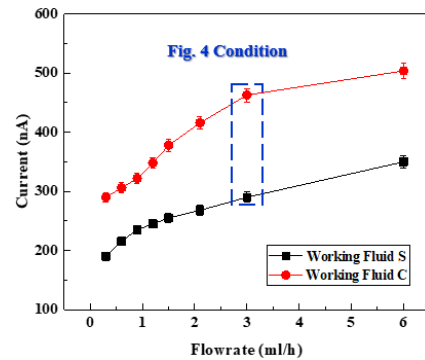


Fig. 5. Dependence of the current associated with the S and C solutions on the flow rate (nozzle diameter: 0.5 mm and NTS: 30 mm).

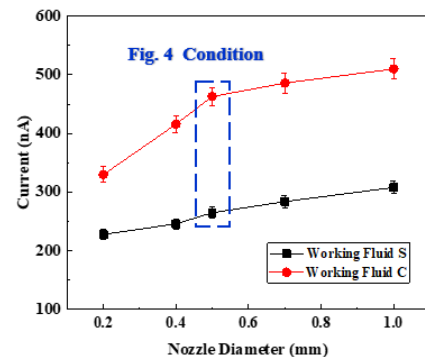


Fig. 6. Dependence of current associated with the S and C solutions on the nozzle diameter (NTS: 30 mm and flow rate: 3.0 mL/h).

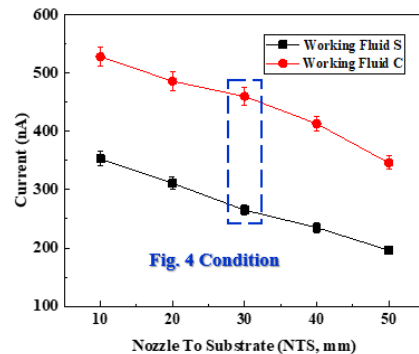


Fig. 7. Current associated with the S and C solutions of NTS (nozzle diameter: 0.5 mm and flow rate: 3.0 mL/h).

visualization data, similar to the results reported by Yunhua *et al.* (2019). During stable cone-shaped spraying, the current was constant regardless of the applied voltage. Furthermore, the current value of the C solution was ~46% higher than that of the S solution. Solution S had a wider range of applied voltages that maintained a constant current during the cone-jet mode. This was because solution C, which had a higher electrical conductivity, could not maintain cone-shaped spraying modes because of the shorter current-relaxation time.

Figure 5 shows the dependence of the current associated with the S and C solutions on the flow rate of the cone jet. Increasing the flow rate resulted in increased current. However, the current tended to saturate to a constant value when the flow rate exceeded 3.0 mL/h. The current value obtained for solution S was ~63% of that obtained for solution C.

Figure 6 shows the dependence of the current on the nozzle diameter associated with the cone-jet mode. As shown in Fig. 6, several nozzle diameters were considered in the experiment. Similar to the trend in Fig. 5, the current value increased with the nozzle diameter. An increase of up to 60% was observed for solution C, whereas an increase of up to 17% was observed for solution S. In addition, the current of the S solution was 58% of that of the C solution. For the C solution, the increase in the amount of current was marginal even when the nozzle diameters were larger than 0.5 mm.

Figure 7 shows the dependence of the current on the NTS for the experimental conditions with several NTS values at intervals of 10 mm. The current associated with the S and C solutions decreased linearly with increasing NTS, owing to a decrease in the strength of the electric field with increasing NTS. The current levels of the S and C solutions decreased by up to 46% and 29%, respectively, with the increase in NTS from 10 mm to 50 mm.

3.3 Droplet Characteristics According to Electro spray Modes

Figures 8 and 9 show the relationship between droplet size and SMD standard deviation based on the electro spray mode. The SMD and SMD standard deviation of the spray mode were determined based on the cone jets of the S and C solutions. Various flow rates (0.3, 2.1, and 6 mL/h) were employed. This allowed the effect of flow rate to be determined (that is, depending on the flow condition, the applied current yielded different spraying modes, as shown in Fig. 3). SMD is proportional to the ratio of the total volume to the total surface area of a group of droplets. This parameter is a measure of the extent of surface penetration required for the atomized liquid to come into contact with the surrounding gas and surface. SMD has been applied to mass transfer and chemical reactions. To verify the differences among spraying modes, the cone jet was set as a reference point for SMD and SMD standard derivation. For both S and C solutions, the SMD values obtained were less than twice those of the cone-jet middle. Among the spray modes of the C solution, the SMDs of the spindle and the unstable modes were 1.65

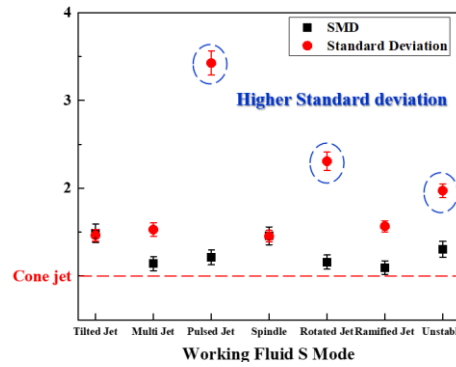


Fig. 8. SMD and SMD standard deviation associated with the S solution mode (nozzle diameter: 1.0 mm, NTS: 30 mm, and flow rate: 3.0 mL/h).

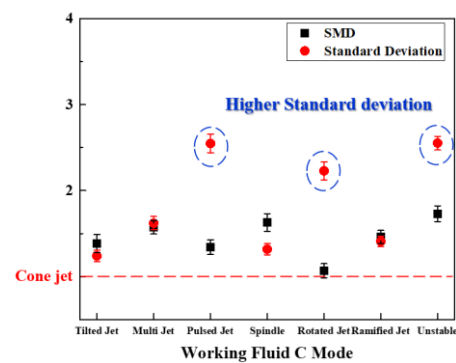


Fig. 9. SMD and SMD standard deviation associated with the C solution mode. (nozzle diameter: 1.0 mm, NTS: 30 mm, and flowrate: 3.0 mL/h).

times that of the cone-jet mode. These SMDs were larger than those of the other spray modes. The large droplets obtained for the spindle and unstable modes were attributed to the lack of jet formation and droplet splitting. Moreover, the standard deviations of the S and C solutions in the pulsed-jet, rotating-jet, and unstable modes were more than twice those in the cone-jet mode. The pulsation phenomenon in the pulsed jet made it impossible to maintain a stable shape of the cone and jet during the spraying mode. Pulsation even caused some droplets to be discharged with a large diameter, similar to the nozzle diameter. An unstable spray pattern was obtained in the unstable mode; the formation of uniform droplets was not observed, suggesting that the distribution was large. This phenomenon occurred in the three modes with non-constant spray patterns. Each pattern changed periodically. In the case of a rotating jet, the rotation results from the effect of the strong electric field of the jet owing to pulsation. In the case of the unstable mode, the spray shape instabilities resulted from a high flow rate and high voltage.

3.4 Droplet Characteristics in a Stable Cone Shape

Figures 10 and 11 show the droplet size in the stable-cone-shape range, and Fig. 12 shows the standard deviation of SMD.

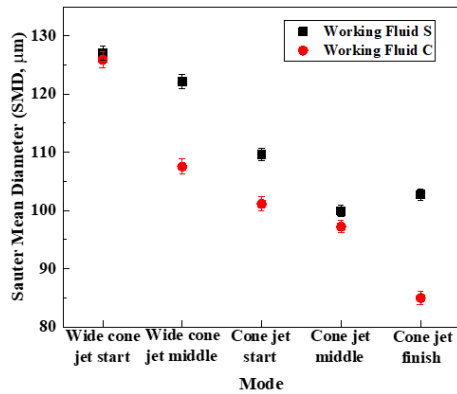


Fig. 10. SMD associated with the cone range (nozzle diameter: 1.0 mm, NTS: 30 mm, and flow rate: 3.0 mL/h).



Fig. 11. Spray image obtained for the cone range (S solution).

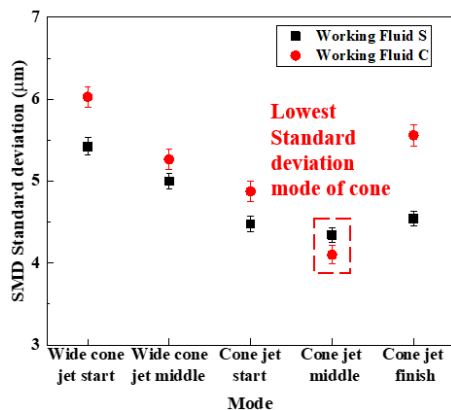


Fig. 12. SMD standard deviation associated with the cone range (nozzle diameter: 1.0 mm, NTS: 30 mm, and flowrate: 3.0 mL/h).

Figure 10 shows the SMD associated with the cone jet. The range encompassing the cone-shaped generation from the wide cone jet to the cone jet was divided into five sections, namely, wide-cone-jet start, wide-cone-jet middle, cone-jet start, cone-jet middle, and cone-jet finish, based on the cone-jet classification. For solution S, the applied voltage values were as follows. Wide-cone-jet start: 6.0 kV,

wide-cone-jet middle: 6.8 kV, cone-jet start: 7.8 kV, cone-jet middle: 8.2 kV, and cone-jet finish: 8.2 kV. The experiment was performed at 8.4 kV. For solution C, the applied voltage values were as follows. Wide-cone-jet start: 5.0 kV, wide-cone-jet middle: 5.7 kV, cone-jet start: 6.4 kV, cone-jet middle: 7.0 kV, and cone-jet finish: 7.6 kV.

For both S and C solutions, the droplet size decreased with the transition from wide cone jet to cone-jet middle. With the further transition to cone-jet finish, for solution C, the droplet size decreased, whereas, for solution S, the droplet was deformed and enlarged. In addition, the tangential velocity of the fluid interface increased owing to the high conductivity of solution C; hence, the droplet size of this solution was smaller than that of solution S.

Figure 11 shows the spray image corresponding to the spray patterns in Fig. 10. As shown in the image, the length (from base to vertex) and thickness (radial direction) of the cone decreased with increasing applied voltage. A cone shape was generated in the cone-jet finish, but the strong voltage occurring in the fluid normal direction led to the movement of the cone and a marginal increase in the droplet size.

Figure 12 shows the standard deviation of SMD under the same experimental conditions as those in Fig. 10. The standard deviations for both the S and C solutions were the smallest in cone-jet middle, where the standard deviation was higher for solution S than for solution C. The standard deviation for both solutions increased upon transition from cone-jet middle to cone-jet finish, where the standard deviation was higher for solution C than for solution S. For the cone-jet finish, the force acting in the direction normal to the fluid interface increased, and hence, the droplets produced by the C solution (unlike the S solution) were nonuniform.

3.5 SMD and SMD Standard Deviation

For solutions S and C, Figs. 13 and 14 show the droplet size variation with an increase in flow rate, and Fig. 15 shows the standard deviation of SMD. Figure 13 shows the effect of the increase in flow rate on SMD. Droplet size formulas from previous studies were employed for comparison with this experiment.

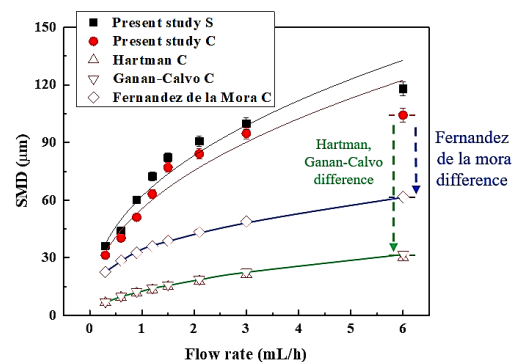


Fig. 13. SMD values of S and C solutions versus flow rate (nozzle diameter: 1.0 mm, NTS: 30 mm, and cone-jet mode).

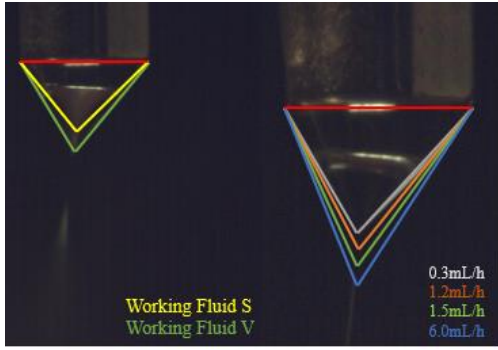


Fig. 14. Spray image obtained for different flow rate values of S solution.

From the droplet size theory proposed by [Fernández De la Mora and Loscertales \(1994\)](#),

$$d = G(\varepsilon)r^* \quad (1)$$

$$r^* = (\varepsilon\varepsilon_0Q/K) 1/3 \quad (2)$$

$$G(\varepsilon) = -10.9\varepsilon^{-6/5} + 4.08\varepsilon^{-1/3} \quad (3)$$

$$G(\varepsilon) = 1.66\varepsilon^{-1/6} \quad (4)$$

From the droplet size theory formulated by [Ganan-Calvo \(1991\)](#),

$$d = 3.78 * 0.6\pi^{-2/3} Q^{1/2} (\frac{\rho\varepsilon_0}{\gamma K})^{1/6} \quad (5)$$

From the droplet size theory formulated by [Hartman et al. \(2000\)](#),

$$d \sim (\frac{\rho\varepsilon_0 Q^3}{\gamma K})^{1/6} \quad (6)$$

According to [Fernández De la Mora and Loscertales \(1994\)](#), experiments were conducted with electrical conductivity values higher than 0.1 uS/cm. In Eq. (1), d is the droplet size, r^* is the electrical characteristic length, and $G(\varepsilon)$ is a function given by Eqs. (3) and (4). [Ganan-Calvo \(1991\)](#) proposed Equation (5), and [Hartman et al. \(2000\)](#) experimentally proposed the diameter equation in Eq. (6). These formulas are based majorly on flow conditions, fluid conductivity, and density.

The droplet size values from the above formulas were up to 4.5 times the SMD values obtained in the present study. This is because the present experiments differed from previous research concerning several conditions, such as nozzle diameter, flow rate, and substrate-nozzle distance. Furthermore, the measured droplet diameter can vary for different measuring systems; this can possibly lead to differences between the experimentally determined droplet diameters and theoretically obtained diameters from the previous studies. The splitting of the liquid jet (owing to the difference in conductivity) could have also contributed to the error.

However, in this experiment, the SMD values obtained for solution C (which had a higher conductivity than solution S) were, on average, 5% smaller than those of solution S. This difference in droplet sizes of the S and C solutions was confirmed using Eqs. (1) – (3), by which the droplet sizes of

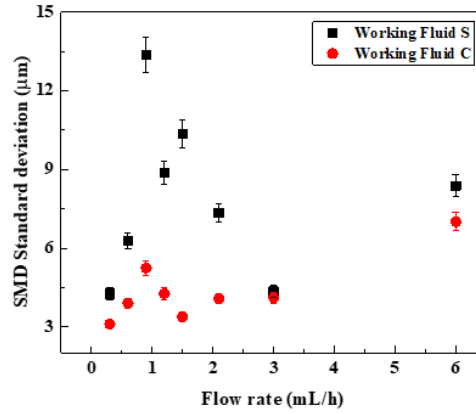


Fig. 15. SMD standard deviation versus flow rate (nozzle diameter: 1.0 mm, NTS: 30 mm, and cone-jet mode).

solution S were 1.17, 2, 1.09, 3, and 1.09 times those of solution C, respectively. Thus, SMD increased with the increase in flow rate.

For the S and C solutions, the length (from base to vertex) of the cone and cone thickness in the cone-jet middle were compared at different flow rates (Fig. 14). For solution S, the thickness and length of the jet increased when the flow rate increased. Owing to the high conductivity of solution C, the jet of solution C was thinner than that of solution S. Thinner jet is estimated the C solution accelerated on the fluid surface more than S solution. Figure 15 shows the SMD standard deviations for solutions S and C at different flow rates. These data were obtained from the same experimental conditions as in Fig. 13. Based on the monodisperse characteristics of the electrospray considered by [Ku and Kim \(2002\)](#), the standard deviation at a specific flow rate was determined. In this experiment, the standard deviation for solution C was smaller than that for solution S. Coalescence was not observed in solution C (with its conductivity higher than that of solution S) even when the droplets were split by the repulsive force of (-) ions on the droplet surface. In addition, the standard deviations for both solutions were small (0.3 mL/h) at the smallest flow rate.

3.6 Current Variation According to SMD

Figure 16 shows the current for different values of SMD. The current value increased with the increase in SMD. For solution C, the increase in the current value with SMD is nonlinear and significant. For a given SMD, compared with solution S, the current was higher for solution C owing to its higher conductivity. Owing to the high conductivity, the charges moved over large distances, and the current increased.

4. CONCLUSION

In this study, the fluid properties and experimental conditions of the electrospray were set as variables, and the spray pattern was analyzed in terms of the droplet size, SMD standard deviation, and current values. The present findings can serve as a reference for experimental studies on electrospray systems.

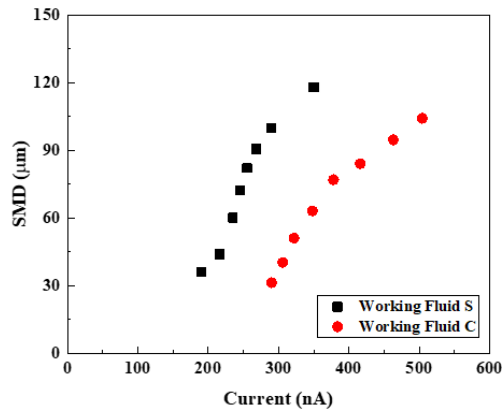


Fig. 16. Current versus SMD associated with each solution (nozzle diameter: 1.0 mm, NTS: 30 mm, and cone-jet mode).

1. The SMD of the cone-jet of solution S was 1.7 times that of solution C. The standard deviation of SMD of pulsed-jet, rotating-jet, and unstable modes were over 2 times that of cone-jet mode.
2. The SMD of solutions S and C in the cone-jet mode decreased with increasing voltage. Moreover, the SMD standard deviation of each solution was the smallest in the cone-jet middle.
3. The SMD value increased with the flow rate and was 5% lower for the high-conductivity solution than for the other solution. The experimentally determined droplet size was up to 4.5 times larger than the theoretical droplet size value from a previous study.
4. The current associated with solution C increased nonlinearly and significantly with an increase in SMD. For a given SMD, the current was larger for solution C than for solution S.

ACKNOWLEDGMENTS

This work was supported by the Human Resources Program in Energy Technology of the Korea Institute of Energy Technology Evaluation and Planning (KETEP) under the auspices of the Ministry of Trade, Industry, & Energy, Republic of Korea (No. 20204010600060).

REFERENCES

- Ariyapadi, S., R. C. Balachandar and F. Berruti (2001). Characterizing spray pulsations using a phase-Doppler particle analyzer. *Industrial & Engineering Chemistry Research* 40(23), 5282-5290.
- Basak, S., D. R. Chen and P. Biswas (2007). Electro spray of ionic precursor solution to synthesize iron oxide nanoparticles: modified scaling law. *Chemical Engineering Science* 62(4), 1263-1268.
- Borra, J. P., D. Camelot K. L. Chou, P. J. Kooyman, J. C. M. Marijnissen and B. Scarlett (1999). Bipolarcoagulation for power production: micro-mixing inside droplets. *Journal of Aerosol Science* 30(7), 945-958.
- Cai, S., Y. Sun, Z. Wang, W. Yang, X. Li and H. Yu (2021) Mechanisms, influencing factors, and applications of electrohydrodynamic jet printing, *Journal of Nanotechnology Reviews*, 10(1), 1046-1078.
- Chen, X., L. Jia, X. Yin, J. Cheng and J. Lu (2005). Spraying modes in coaxial jet electro spray with outer driving liquid. *Physics of Fluids* 17(3), 032101.
- De la Mora, J. F. and I. G. Loscertales (1994). The current emitted by highly conducting Taylor cones. *Journal of Fluid Mechanics* 260, 155-184.
- Eduardo, C. O., K. Aravinda and K. Ranganathan (2020). Non-dimensional groups for electro spray modes of highly conductive and viscous nanoparticle suspensions. *Scientific Reports* 10(1), 4405.
- Gamero-Castano, M. and V. Hruby (2001). Electro spray as a source of nanoparticles for efficient colloid thrusters. *Journal of Propulsion and Power* 17(5).
- Gañán-Calvo, A. M. (1991). Cone-jet analytical extension of Taylor's electrostatic solution and the asymptotic universal scaling laws in electro spraying. *Physical Review Letters* 79(2), 217-220.
- Hartman, R. P. A., D. J. Brunner, D. M. A. Camelot, J. C. M. Marijnissen and B. Scarlett (2000). Jet break-up in electrohydrodynamic atomization in the cone-jet mode. *Journal of Aerosol Science* 31(1), 65-95.
- Jaworek, A. and A. Krupa (1996). Generation and characteristics of the precession mode of EHD spraying. *Journal of Aerosol Science* 27(1), 75-82.
- Jayasinghe, S. N. and M. J. Edirisinghe (2002). Effect of viscosity on the size of relics produced by electrostatic atomization. *Journal of Aerosol Science* 33(10), 1379-1388.
- Jeong, J. H., H. S. Choi, K. S. Park, H. S. Kim, J. Y. Choi, I. Y. Park and S. S. Lee (2020). Polymer micro-atomizer for water electro spray in the cone jet mode. *Polymer* 194(24), 122405.
- Kim, J. Y. and J. G. Hong (2020). Spray Characteristics according to Fluid Properties and Electric Parameters of Electro spray. *Journal of ilass-korea* 25(2), 81-88.
- Kim, J. Y., S. J. Lee, G. Y. Baik and J. G. Hong (2021). Viscosity Effect on the Electro spray Characteristics of Droplet Size and Distribution. *ACS OMEGA* 6(44), 29724-29734.
- Kim, J. Y., S. J. Lee., G. W. Baik and J. G. Hong (2021). Effects of working fluids on spray modes and atomization characteristics in

- electrospray. *Journal of the Korean Society for Precision Engineering* 38(1), 61-68.
- Ku, B. K. and S. S. Kim (2002). Electro spray characteristics of highly viscous liquids. *Journal of Aerosol Science* 33(10), 1361-1378.
- Ku, K. W., J. G. Hong and C. W. Park (2015). Effect of assist-air of twin fluid atomizer on urea thermal decomposition. *Atomization Sprays* 25, 895-915.
- Laonual, Y. (2006). *Optical investigation of evaporating spray*. PhD Thesis, Imperial College London, London, UK.
- Lefebvre, H. and V. G. McDonell (2017). *Atomization and sprays*, Second Edition, Begell House, Boca Raton, USA.
- Morad, M. R., A. Rajabi, M. Razavi and S. R. P. A. Sereshkeh (2016). very stable high throughput Taylor cone-jet in electrohydrodynamics, *Scientific Reports* 6, 38509.
- Rahman, K., K. Ali, N. M. Muhammad, M. T. Hyun and K. H. Choi (2013). Fine resolution drop-on-demand electrohydrodynamic patterning of conductive silver tracks on glass substrate. *Applied physics A* 111(2).
- Rahmanpour, M. and R. Ebrahimi (2017). Numerical Simulation of Highly Charged Droplets Dynamics with Primary Break-up in Electro spray at Sub Rayleigh Limit. *Journal of Applied Fluid Mechanics* 10(2), 541-550.
- Sugiyama, H., H. Gura and Y. Otsubo (2011). Fluid Devices by the Use of Electrohydrodynamic Effects of Water, *Journal of Applied Fluid Mechanics* 4(1), 27-33.
- Suhendi, A., M. M. Munir, A. B. Suryamas, A. B. D. Nandiyanto, T. Ogi and K. Okuyama (2013). Control of cone-jet geometry during electro spray by an electric current. *Advanced Powder Technology* 24(2), 532-536.
- Sultan, F., N. Ashgriz, D. R. Gueldenbecher, P. E. Sojka, D. R. Gueldenbecher., P. E. Sojka. (2011). *Handbook of Atomization and Sprays*, Springer, New York, USA.
- Tang, K. and A. Gomez (1996). Monodisperse electro sprays of low electric conductivity liquids in the cone-jet mode. *Journal of Colloid and Interface Science* 184(2), 500-511.
- Tara Liyanage, O., M. R. Brantley, E. I. Calixte, T. Solouki, K. L. Shuford and E. S. Gallagher (2018). Characterization of electro spray ionization (ESI) parameters on in-ESI hydrogen/deuterium exchange of carbohydrate-metal ion adducts. *Journal of the American Society for Mass Spectrometry* 30(2), 235-247.
- Taylor, G. (1964). Disintegration of water drops in an electric field. *Proceedings of the Royal Society of Edinburgh Section A Mathematics*, 280(1382), 383-397.
- Ting, S., Z. Leilei, L. Guangbin, J. R. Cynthia, T. Xiezheng and X. Ronald (2013). Experimental design and instability analysis of coaxial electro spray process for microencapsulation of drugs and imaging agents. *Journal of Biomedical Optics* 18(7), 075003.
- Wang, K. and J. P. W. Stark (2010). Direct fabrication of electrically functional microstructures by fully voltage-controlled electrohydrodynamic jet printing of silver nano-ink. *Applied Physics A* 99(4), 763-766.
- Wang, X., J. Lin, J. Jiang, S. Guo, W. Li and G. Zheng (2018). Continuous Near-Field Electro spraying Using a Glass Capillary Nozzle. *Micromachines* 9(2), 56.
- Yazdekhasti, A., A. Pishavar and A. Valipouri (2019). Investigating the effect of electrical conductivity on electro spray modes. *Experimental Thermal and Fluid Science* 100(1), 328-336.
- Yunhua, G., J. Zhengwei, L. Haige, L. Yanlai, C. Xiaowen, S. Yanling, Y. Yuying and Y. A. Yunfei (2019). Comparative study on droplet characteristics and specific charge of ethanol in two small-scale electro spray systems. *Scientific Reports* 9, 18791.